ed locally within the receptive field of a DSGC (*2*), the asymmetric inhibitory inputs must affect only a local region ("subunit") of the dendritic tree. This is consistent with the postsynaptic inhibition being of a shunting, and thus divisive, nature (*15*). Moreover, the dendritic architecture of the DSGCs appears to provide an appropriate substrate for such postsynaptic interactions. In both the On and Off sublaminae of the inner plexiform layer, dendrites of all orders give rise to thin terminal branches, which cover the dendritic field in a space-filling lattice (*16, 17*). These terminal dendrites provide sites away from the main dendritic trunks where excitatory and inhibitory inputs may interact locally. Nevertheless, postsynaptic inhibition could produce a distinct asymmetry between the preferred and null sides of the receptive field. When a null-direction stimulus enters the null side of the dendritic field, much of the inhibition impinges proximally, between the excitatory inputs and the cell body. When the stimulus crosses to the preferred side, much of the inhibition impinges more distally to the excitatory inputs and may extend beyond the edge of the dendritic field. Thus, a functional asymmetry may arise because modeling studies predict that an inhibitory shunt located proximally to the excitatory input is much more effective than a similar input located distally (*10*). This arrangement might produce aberrant responses to some moving stimuli and may explain the presence of a nondirectional zone on the preferred side of DSGCs, covering as much as 20 to 25% of the receptive field (*2, 18*).

Our study demonstrates a major role for postsynaptic dendritic processing in a clearly defined and well-characterized neuronal computation, thus providing strong support for the theoretical studies that advocated such interactions (*9, 10, 15*). Many questions about the cellular mechanism of direction selectivity in the retina remain to be answered (*5*); the most important ones concern the identity of the GABAergic amacrine cells that mediate the null-direction inhibition and the manner in which they selectively contact different subtypes of DSGCs with different preferred directions. The results of this study, showing that the null-direction inhibition acts directly on the ganglion cell dendrites, provide a critical guidepost for future investigations.

References and Notes

1. H. B. Barlow, R. M. Hill, W. R. Levick, *J. Physiol.* **173**, 377 (1964).
2. H. B. Barlow and W. R. Levick, *J. Physiol.* **178**, 477 (1965).
3. C. W. Oyster and H. B. Barlow, *Science* **155**, 841 (1967).
4. F. R. Amthor and N. M. Grzywacz, *J. Neurophysiol.* **69**, 2174 (1993).
5. S. He and R. H. Masland, *Nature* **389**, 378 (1997).
6. H. J. Wyatt and N. D. Daw, *Science* **191**, 204 (1976).
7. M. Ariel and N. W. Daw, *J. Physiol.* **324**, 161 (1982).
8. C. A. Kittila and S. C. Massey, *J. Neurophysiol.* **77**, 675 (1997).
9. V. Torre and T. Poggio, *Proc. R. Soc. London Ser. B* **202**, 409 (1978).
10. C. Koch, T. Poggio, V. Torre, *Philos. Trans. R. Soc. London Ser. B* **298**, 227 (1982).
11. The techniques for making patch recordings from retinal ganglion cells followed those of Taylor and Wässle (*19*). Retinas from dark-adapted pigmented rabbits were isolated under infrared illumination (940 nm) and then flat-mounted with the photoreceptors down in a recording chamber on the fixed stage of an upright microscope. The preparation was continuously superfused (3 ml/min) with oxygenated Ames medium at 35° ± 0.2°C. On-Off DSGCs were initially targeted under infrared illumination as having a round medium-sized soma (~15 μm in diameter) with a crescent-shaped nucleus (*17*). The overlying inner limiting membrane and surrounding Müller cell end feet were microdissected away, and a patch electrode (3 to 7 megohms) was applied to the exposed soma. Membrane voltage or membrane current was recorded with an Axopatch 200B amplifier in the whole-cell recording configuration. Signals were filtered at 2 kHz (eight-pole Bessel filter) and sampled at 5 to 10 kHz.
12. Visual stimuli were generated on a Barco display monitor and projected onto the back focal plane of a ×40 (0.8 numerical aperture) water-immersion microscope objective, which focused the image onto the photoreceptor outer segments. The ×40 objective illuminated a region of retina with a diameter of ~500 μm. The stimulus consisted of a light bar, which was 250 μm wide and at least 500 μm long, moving across the stimulus region at 1 mm/s on a trajectory parallel to the long axis. The length of the bar ensured that the leading and trailing edges did not appear within the stimulus region simultaneously, thus allowing for adequate separation of the leading-edge (On) and trailing-edge (Off) responses. In Figs. 2A; 3, A and B; and 4, A and B, the stimulus timing is shown by a light bar beneath the records; the start and finish of the white bar mark the entry into the stimulus region of the leading and trailing edges, respectively.
13. P. L. Marchiafava, *Vision Res.* **19**, 1203 (1979).
14. The external solution was Ames medium, a bicarbonate-buffered physiological saline equilibrated to pH 7.45 with 95% O_2/5% CO_2 and containing a full complement of amino acids, vitamins, and glucose. The ionic composition of the external solution was as follows: 120 mM NaCl, 23 mM $NaHCO_3$, 3.1 mM KCl, 1.15 mM $CaCl_2$, and 1.2 mM $MgCl_2$. Recording electrodes were filled with a solution (pH 7.4) containing 120 mM K-gluconate, 5 mM NaCl, 5 mM KCl, 5 mM Hepes, 1 mM $MgCl_2$, 1 mM EGTA, 1 mM adenosine 5′-triphosphate, and 0.1 mM guanosine 5′-triphosphate. For the voltage-clamp recordings shown in Fig. 3, potassium was replaced with cesium. For the high-chloride experiments shown in Fig. 4, K-gluconate was replaced with CsCl. In order to work quickly to observe the changes resulting from chloride loading, the command potential for the voltage clamp was set to –30 mV before break-in, and recording commenced immediately upon rupture of the membrane beneath the recording electrode.
15. C. Koch, T. Poggio, V. Torre, *Proc. Natl. Acad. Sci. U.S.A.* **80**, 2799 (1983).
16. C. W. Oyster, F. R. Amthor, E. S. Takahashi, *Vision Res.* **33**, 579 (1993).
17. D. I. Vaney, *J. Neurosci.* **14**, 6301 (1994).
18. S. He, Z. F. Jin, R. H. Masland, *J. Neurosci.* **19**, 8049 (1999).
19. W. Taylor and H. Wässle, *Eur. J. Neurosci.* **7**, 2308 (1995).

20. This work was supported by a National Health and Medical Research Council project grant to D.I.V. and W.R.T. and through recurrent funding by the John Curtin School of Medical Research to W.R.T. We thank J. M. Bekkers, P. Sah, G. Stuart, and B. Walmsley for helpful comments on the manuscript.

14 April 2000; accepted 11 August 2000

Failure to Regulate TNF-Induced NF-κB and Cell Death Responses in A20-Deficient Mice

Eric G. Lee,* David L. Boone,* Sophia Chai, Shon L. Libby, Marcia Chien, James P. Lodolce, Averil Ma†

A20 is a cytoplasmic zinc finger protein that inhibits nuclear factor κB (NF-κB) activity and tumor necrosis factor (TNF)–mediated programmed cell death (PCD). TNF dramatically increases A20 messenger RNA expression in all tissues. Mice deficient for A20 develop severe inflammation and cachexia, are hypersensitive to both lipopolysaccharide and TNF, and die prematurely. A20-deficient cells fail to terminate TNF-induced NF-κB responses. These cells are also more susceptible than control cells to undergo TNF-mediated PCD. Thus, A20 is critical for limiting inflammation by terminating TNF-induced NF-κB responses in vivo.

During inflammatory responses, TNF and interleukin-1 (IL-1) signals activate NF-κB, which regulates the transcription of other proinflammatory genes. The factors that limit these responses are poorly understood. A20 is a cytoplasmic protein thought to be expressed predominantly in lymphoid tissues, and heterologously expressed A20 can inhibit TNF-induced NF-κB and PCD responses in cell lines (*1–4*). A20 binding to TNF receptor–associated factor-2 (TRAF2), inhibitor of NF-κB kinase gamma (IKKγ), and/or A20-binding inhibitor of NF-κB activation (ABIN) suggest potential mechanisms by which A20 could regulate TNF receptor signals (*5–7*);

Department of Medicine, The University of Chicago, 5841 South Maryland Avenue, MC 6084, Chicago, IL 60637, USA.

*These authors contributed equally to this work.
†To whom correspondence should be addressed. E-mail: ama@medicine.bsd.uchicago.edu

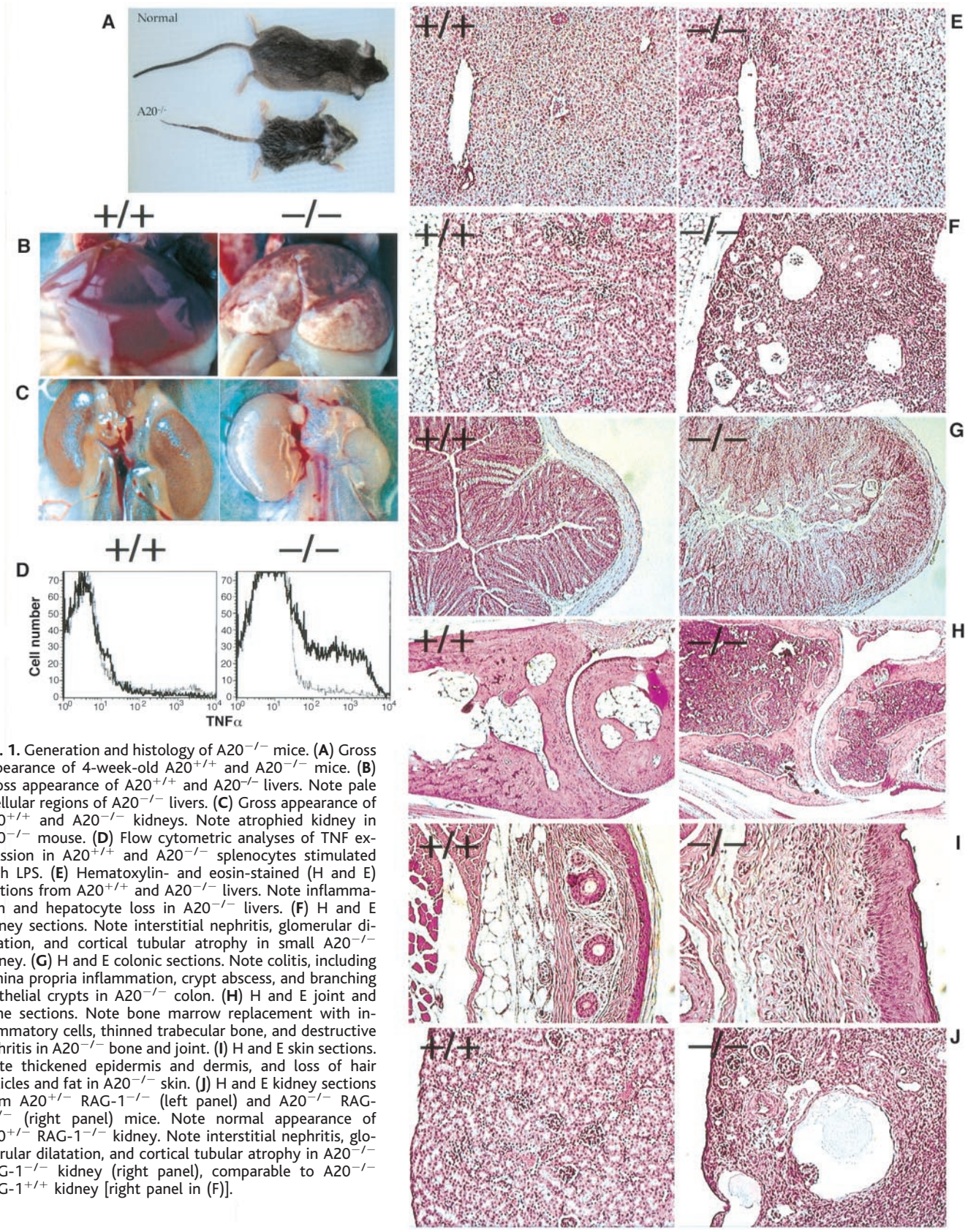

Fig. 1. Generation and histology of A20$^{-/-}$ mice. (**A**) Gross appearance of 4-week-old A20$^{+/+}$ and A20$^{-/-}$ mice. (**B**) Gross appearance of A20$^{+/+}$ and A20$^{-/-}$ livers. Note pale acellular regions of A20$^{-/-}$ livers. (**C**) Gross appearance of A20$^{+/+}$ and A20$^{-/-}$ kidneys. Note atrophied kidney in A20$^{-/-}$ mouse. (**D**) Flow cytometric analyses of TNF expression in A20$^{+/+}$ and A20$^{-/-}$ splenocytes stimulated with LPS. (**E**) Hematoxylin- and eosin-stained (H and E) sections from A20$^{+/+}$ and A20$^{-/-}$ livers. Note inflammation and hepatocyte loss in A20$^{-/-}$ livers. (**F**) H and E kidney sections. Note interstitial nephritis, glomerular dilatation, and cortical tubular atrophy in small A20$^{-/-}$ kidney. (**G**) H and E colonic sections. Note colitis, including lamina propria inflammation, crypt abscess, and branching epithelial crypts in A20$^{-/-}$ colon. (**H**) H and E joint and bone sections. Note bone marrow replacement with inflammatory cells, thinned trabecular bone, and destructive arthritis in A20$^{-/-}$ bone and joint. (**I**) H and E skin sections. Note thickened epidermis and dermis, and loss of hair follicles and fat in A20$^{-/-}$ skin. (**J**) H and E kidney sections from A20$^{+/-}$ RAG-1$^{-/-}$ (left panel) and A20$^{-/-}$ RAG-1$^{-/-}$ (right panel) mice. Note normal appearance of A20$^{+/-}$ RAG-1$^{-/-}$ kidney. Note interstitial nephritis, glomerular dilatation, and cortical tubular atrophy in A20$^{-/-}$ RAG-1$^{-/-}$ kidney (right panel), comparable to A20$^{-/-}$ RAG-1$^{+/+}$ kidney [right panel in (F)].

however, the functions of A20 in vivo are unknown. Thus, we generated A20-deficient (A20$^{-/-}$) mice by gene targeting (*8*).

A20$^{+/-}$ mice appeared normal without evidence of pathology. A20$^{-/-}$ mice were born from interbred A20$^{+/-}$ mice in Mendelian ratios, demonstrating that A20 is not required for embryonic survival. A20$^{-/-}$ pups were runted as early as 1 week of age

and began to die shortly thereafter (Fig. 1A). Gross and histological examination of 3- to 6-week-old A20$^{-/-}$ mice revealed severe inflammation and tissue damage in multiple organs, including livers (Fig. 1, B and E), kidneys (Fig. 1, C and F), intestines (Fig. 1G), joints, and bone marrow (Fig. 1H). Flow cytometric analysis of A20$^{-/-}$ spleens and livers revealed increased numbers of activated lymphocytes (CD3^{+} CD44^{+}), granulocytes (CD3^{-} Gr-1^{+} Mac-1^{+}), and macrophages (CD3^{-} Mac-1^{+}) (*8*). Double mutant A20$^{-/-}$ recombinase-activating gene-1–deficient (RAG-1$^{-/-}$) mice developed granulocytic infiltration, cachexia, and premature death at a similar frequency and severity to A20$^{-/-}$ RAG-1$^{+/-}$ littermates (Fig. 1, F and J), indicating that lymphocytes are not required for the inflammation seen in A20$^{-/-}$ mice. Finally, skin sections revealed thickened epidermal and dermal layers without inflammation (Fig. 1I). Thus, A20 is essential for preventing spontaneous innate immune cell–mediated inflammation and tissue destruction, as well as regulating skin differentiation.

The role of A20 in regulating inflammation was further evaluated by examining the sensitivity of A20$^{-/-}$ mice to lipopolysaccharide (LPS). All A20$^{-/-}$ mice died within 2 hours of injection of 5 mg LPS per kg of body weight, whereas A20$^{+/+}$ and A20$^{+/-}$ mice given 5, 12, or 25 mg/kg LPS survived without significant morbidity (Table 1). This hypersensitivity to LPS was correlated with increased numbers of A20$^{-/-}$ splenocytes expressing TNF after LPS stimulation (Fig. 1D). In addition, A20$^{-/-}$ mice were highly susceptible to low doses of TNF, as all A20$^{-/-}$ mice died within 2 hours of injection of 0.1 mg/kg TNF, whereas A20$^{+/+}$ and A20$^{+/-}$ mice given 0.1, 0.2, or 0.4 mg/kg TNF survived (Table 1). Consistent with the marked susceptibility of A20$^{-/-}$ mice to TNF, A20 mRNA expression was dramatically increased by TNF in all tissues examined from normal mice (Fig. 2A). Thus, A20 may protect mice from inflammatory mediators by regulating TNF responses in multiple cell types.

The hypersensitivity of A20$^{-/-}$ mice to TNF may be due in part to the capacity of A20 to regulate PCD (*1, 4*). Thymocytes constitutively express both TNF (*9*) and A20 mRNA (*4*). Although corticosteroids, γ-irradiation, and Fas receptor ligation killed comparable numbers of A20$^{+/-}$ and A20$^{-/-}$ thymocytes, A20$^{-/-}$ thymocytes were more sensitive to TNF, both in the presence and absence of cycloheximide (Fig. 2B). TNF-mediated PCD was blocked by the caspase inhibitor ZVAD-fmk, confirming that caspase-dependent pathways kill these

Table 1. A20$^{-/-}$ mice succumb to sublethal doses of LPS and TNF. Indicated doses of LPS or TNF were given to 17- to 20-day-old A20$^{+/+}$ and A20$^{-/-}$ littermates. Numbers of mice surviving at 2 hours are indicated over the numbers of mice injected. Surviving mice were observed for 6 hours further to rule out delayed effects of LPS or TNF.

Genotype	LPS (mg/kg)			TNF (mg/kg)		
	5	12.5	25	0.1	0.2	0.4
+/+, +/−	4/4	4/4	4/4	5/5	2/2	2/2
−/−	0/4	–	–	0/4	–	–

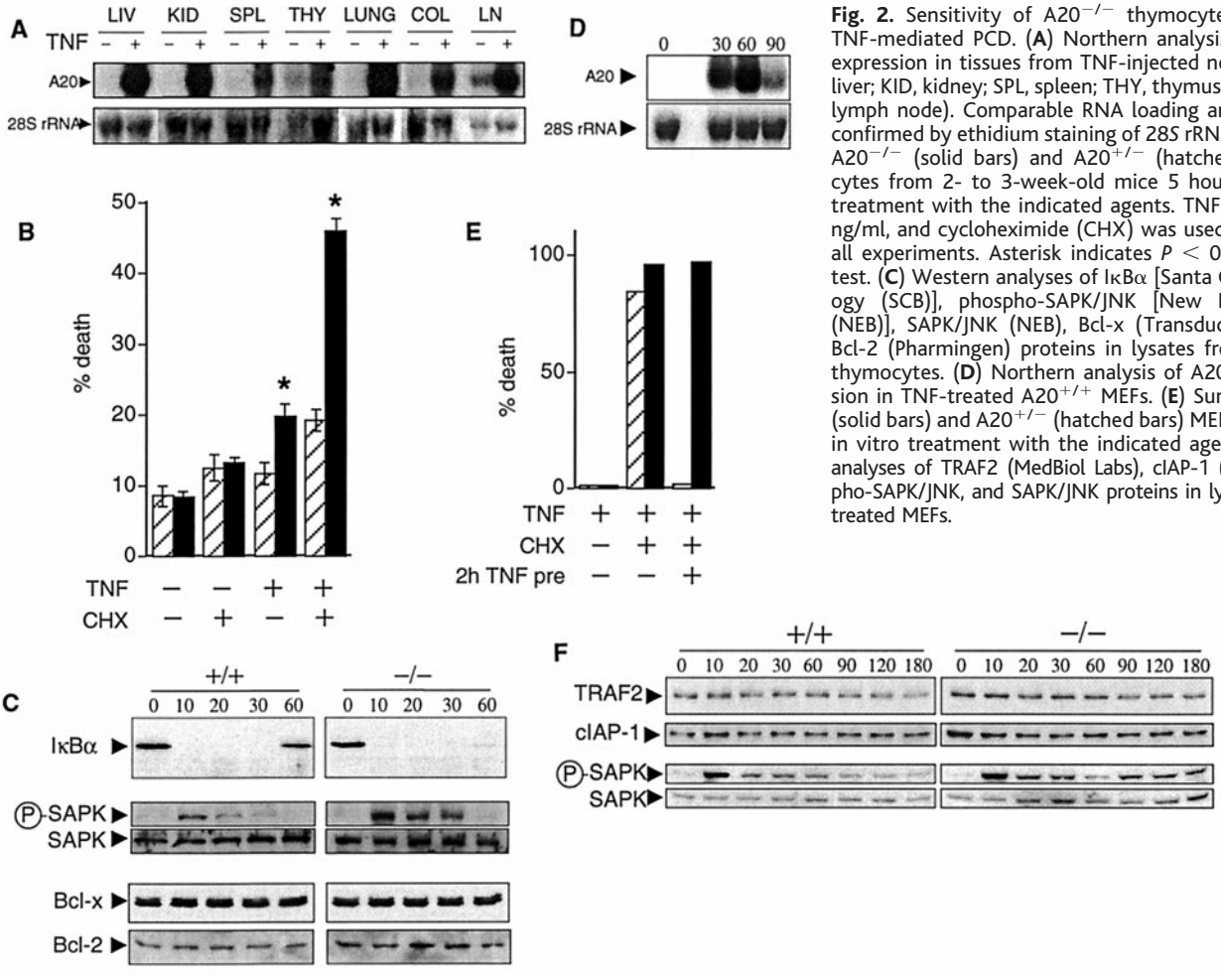

Fig. 2. Sensitivity of A20$^{-/-}$ thymocytes and MEFs to TNF-mediated PCD. (**A**) Northern analysis of A20 mRNA expression in tissues from TNF-injected normal mice (LIV, liver; KID, kidney; SPL, spleen; THY, thymus; COL, colon; LN, lymph node). Comparable RNA loading and integrity was confirmed by ethidium staining of 28*S* rRNA. (**B**) Survival of A20$^{-/-}$ (solid bars) and A20$^{+/-}$ (hatched bars) thymocytes from 2- to 3-week-old mice 5 hours after in vitro treatment with the indicated agents. TNF was used at 10 ng/ml, and cycloheximide (CHX) was used at 10 μg/ml in all experiments. Asterisk indicates $P < 0.001$ by Tukey's test. (**C**) Western analyses of IκBα [Santa Cruz Biotechnology (SCB)], phospho-SAPK/JNK [New England Biolabs (NEB)], SAPK/JNK (NEB), Bcl-x (Transduction Labs), and Bcl-2 (Pharmingen) proteins in lysates from TNF-treated thymocytes. (**D**) Northern analysis of A20 mRNA expression in TNF-treated A20$^{+/+}$ MEFs. (**E**) Survival of A20$^{-/-}$ (solid bars) and A20$^{+/-}$ (hatched bars) MEFs 10 hours after in vitro treatment with the indicated agents. (**F**) Western analyses of TRAF2 (MedBiol Labs), cIAP-1 (Trevigen), phospho-SAPK/JNK, and SAPK/JNK proteins in lysates from TNF-treated MEFs.

cells. Levels of the survival proteins Bcl-2 and Bcl-x were comparable in $A20^{-/-}$ and $A20^{+/+}$ thymocytes (Fig. 2C). Both stress-activated protein kinase (SAPK) (or c-Jun N-terminal kinase, JNK) phosphorylation and inhibitor of κB alpha (IκBα) degradation were seen in TNF-treated $A20^{-/-}$ thymocytes (Fig. 2C), suggesting that the synthesis of survival proteins by SAPK/JNK- and NF-κB–dependent pathways was intact (*10–13*). Thus, A20 protects thymocytes from TNF-mediated PCD independently of protein synthesis or other known thymocyte survival factors.

The ability of A20 to regulate TNF responses was further examined in mouse embryonic fibroblasts (MEFs), which express negligible A20 mRNA at rest and dramatically increase levels of A20 mRNA expression after TNF treatment (Fig. 2D). While pretreatment of normal cells with TNF leads to the synthesis of survival proteins which protect these cells from subsequent TNF plus cycloheximide (*14*), $A20^{-/-}$ MEFs universally died despite TNF pretreatment (Fig. 2E). Activation of both SAPK/JNK and NF-κB pathways and similar levels of the survival proteins cellular inhibitor of apoptosis-1 (c-IAP1) and TRAF2 were seen in TNF-treated $A20^{+/+}$ and $A20^{-/-}$ MEFs (Fig. 2F and Fig. 3A). Thus, TNF-mediated synthesis of presumably all NF-κB– and SAPK/JNK-dependent survival proteins (*15*) except A20 was insufficient to protect $A20^{-/-}$ MEFs from PCD mediated by TNF plus cycloheximide.

A20 inhibits NF-κB activation (*2*), and dysregulated NF-κB activity leads to inflammation and premature death in $I\kappa B\alpha^{-/-}$ mice (*16*). Moreover, the perturbed skin differentiation seen in $A20^{-/-}$ mice resembles the skin of $I\kappa B\alpha^{-/-}$ mice (*16*). Thus, the pathogenesis of $A20^{-/-}$ mice may be due in part to dysregulated NF-κB activity. Repeated TNF treatment of normal MEFs caused IκBα degradation and NF-κB binding to DNA, followed by down-regulation of NF-κB binding and reaccumulation of IκBα protein by 60 min (Fig. 3, A and B). In contrast, NF-κB binding to DNA persisted and IκBα protein was not detected in $A20^{-/-}$ MEFs from 60 to 180 min of TNF treatment (Fig. 3, A and B). IκBα mRNA levels, transcriptionally enhanced by NF-κB (*17*), increased in response to TNF in both $A20^{+/+}$ and $A20^{-/-}$ MEFs, indicating that the failure of $A20^{-/-}$ MEFs to reaccumulate IκBα protein was not due to a failure to express IκBα mRNA (Fig. 3C). Addition of the proteasome inhibitor MG-132 to MEFs 15 min after TNF treatment caused $A20^{-/-}$ MEFs to regain normal levels of IκBα protein (Fig. 3D, top panels), suggesting that the lack of IκBα protein reaccumulation in TNF-treated $A20^{-/-}$ MEFs was due to rapid degradation of newly synthesized IκBα protein, rather than the failure of these cells to translate IκBα mRNA. IκBα protein that reaccumulated in MG-132–treated $A20^{-/-}$ but not $A20^{+/+}$ MEFs was phosphorylated (Fig. 3D, bottom panels), suggesting that persistent IKK (a multimeric complex comprising IKKα, IKKβ, and IKKγ) activity caused rapid phosphorylation of newly synthesized IκBα protein in TNF-treated $A20^{-/-}$ MEFs. Direct measurement of IKK activity in lysates from TNF-treated MEFs confirmed this suggestion (Fig. 3E). Therefore, synthesis of IκBα mRNA and IκBα protein is insufficient to terminate NF-κB signals in the absence of A20.

Finally, we examined the role of A20 in regulating NF-κB responses to IL-1β. NF-κB activity increased and decreased normally and IκBα protein reaccumulated normally in IL-1β–treated $A20^{-/-}$ MEFs (Fig. 3F). Thus, although prior studies suggested that heterologous A20 can inhibit IL-1β–induced NF-κB responses (*5, 18*), A20 is not essential for terminating these responses. Moreover, it is likely that A20 inhibits TNF activation of the NF-κB pathway upstream of IKKγ, since IKKγ is required for both IL-1β– and TNF-induced NF-κB activation (*19*).

A20 is a dynamically regulated and pleiotropically expressed gene that is required for negatively regulating NF-κB responses in vivo. A20 may also regulate TNF-induced SAPK/JNK and PCD responses. The ability of A20 to inhibit TNF- but not IL-1β–induced NF-κB signals suggests these signals

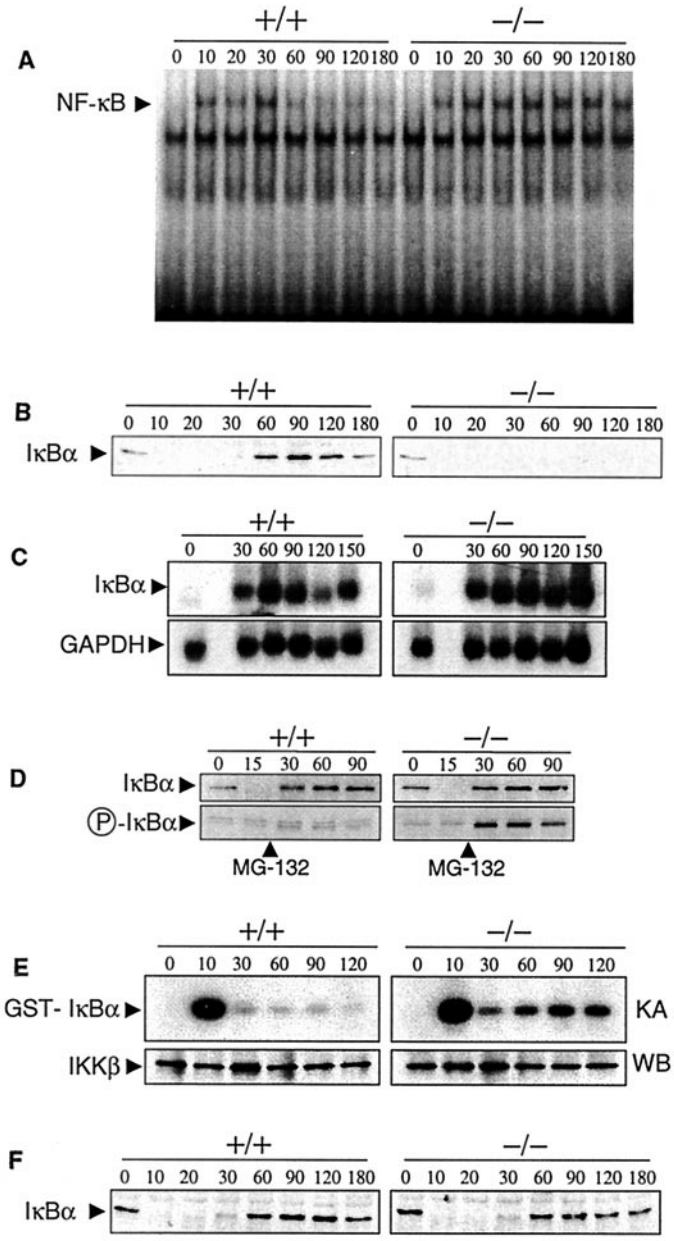

Fig. 3. Prolonged NF-κB responses to TNF in $A20^{-/-}$ MEFs. Electrophoretic mobility-shift assay (EMSA), Western, and Northern blot analyses of $A20^{+/+}$ and $A20^{-/-}$ MEFs treated repeatedly with TNF and harvested at the indicated time points. (**A**) EMSA analyses of NF-κB activity, using an NF-κB consensus oligonucleotide (SCB). (**B**) Western blot analysis of IκBα expression. (**C**) Northern blot analyses of IκBα and glyceraldehyde phosphate dehydrogenase (GAPDH) mRNA expression in MEFs. (**D**) Western blot analyses of IκBα and phospho-IκBα expression after proteasome inhibition. (**E**) IKK kinase assay of TNF-treated MEFs. Total cell lysates from repeatedly TNF-treated MEFs were immunoprecipitated with an anti-IKKγ antibody (SCB), and kinase activity was assessed using a GST-IκBα (1-54) substrate (upper panels). Comparable IKKβ protein in immunoprecipitated samples confirmed by Western analysis (lower panels). (**F**) Western analysis of IκBα expression in IL-1β–treated MEFs.

can be differentially regulated in vivo. The rapid expression of A20 is essential for limiting inflammatory responses and the damage those responses cause in multiple tissues.

References and Notes

1. A. W. Opipari Jr., H. M. Hu, R. Yabkowitz, V. M. Dixit, *J. Biol. Chem.* **267**, 12424 (1992).
2. J. T. Cooper *et al.*, *J. Biol. Chem.* **271**, 18068 (1996).
3. A. W. Opipari Jr., M. S. Boguski, V. M. Dixit, *J. Biol. Chem.* **265**, 14705 (1990).
4. M. Tewari *et al.*, *J. Immunol.* **154**, 1699 (1995).
5. H. Y. Song, M. Rothe, D. V. Goeddel, *Proc. Natl. Acad. Sci. U.S.A.* **93**, 6721 (1996).
6. S. Zhang, A. Kovalenko, G. Cantarella, D. Wallach, *Immunity* **12**, 301 (2000).
7. K. Heyninck *et al.*, *J. Cell Biol.* **145**, 1471 (1999).
8. Supplemental material is available at www.sciencemag.org/feature/data/1053996.shl
9. B. P. Giroir, T. Brown, B. Beutler, *Proc. Natl. Acad. Sci. U.S.A.* **89**, 4864 (1992).
10. A. A. Beg and D. Baltimore, *Science* **274**, 782 (1996).
11. C. Y. Wang, M. W. Mayo, A. S. Baldwin Jr., *Science* **274**, 784 (1996).
12. D. J. Van Antwerp, S. J. Martin, T. Kafri, D. R. Green, I. M. Verma, *Science* **274**, 787 (1996).
13. Z. G. Liu, H. Hsu, D. V. Goeddel, M. Karin, *Cell* **87**, 565 (1996).
14. G. H. W. Wong and D. Goeddel, *J. Immunol.* **152**, 1751 (1994).
15. C. Y. Wang, M. W. Mayo, R. G. Korneluk, D. V. Goeddel, A. S. Baldwin Jr., *Science* **281**, 1680 (1998).
16. A. A. Beg, W. C. Sha, R. T. Bronson, D. Baltimore, *Genes Dev.* **9**, 2736 (1995).
17. S. C. Sun, P.A. Ganchi, D.W. Ballard, W. C. Greene, *Science* **259**, 1912 (1993).
18. M. Jaattela, H. Mouritzen, F. Elling, L. Bastholm, *J. Immunol.* **156**, 1166 (1996).
19. D. Rudolph *et al.*, *Genes Dev.* **14**, 854 (2000).

20. We thank V. Dixit for helpful suggestions and for providing the A20 cDNA; B. Malynn, M. Peter, and G. Franzoso for helpful suggestions and for critically reading the manuscript; A. Lin for valuable advice with IKKγ kinase assays; and F. Jackson for administrative assistance. Supported by NIH grants RO1 DK52751 and AI45860 (to A.M.), the Crohn's and Colitis Foundation of America (to A.M.), the Mr. and Mrs. Arthur Edelstein fluorescence-activated cell sorting facility, the Martin Boyer Genetics Laboratories, and the Gastrointestinal Research Foundation. A.M. is a Cancer Research Institute Scholar. E.G.L. and J.P.L. are supported by training grant 5T32GM07183. S.L.L. is supported by training grant T32GM07839.

20 March 2000; accepted 14 August 2000

A Specificity-Enhancing Factor for the ClpXP Degradation Machine

Igor Levchenko,[1,2] Meredith Seidel,[1,2] Robert T. Sauer,[1] Tania A. Baker[1,2]*

Events that stall bacterial protein synthesis activate the ssrA-tagging machinery, resulting in resumption of translation and addition of an 11-residue peptide to the carboxyl terminus of the nascent chain. This ssrA-encoded peptide tag marks the incomplete protein for degradation by the energy-dependent ClpXP protease. Here, a ribosome-associated protein, SspB, was found to bind specifically to ssrA-tagged proteins and to enhance recognition of these proteins by ClpXP. Cells with an *sspB* mutation are defective in degrading ssrA-tagged proteins, demonstrating that SspB is a specificity-enhancing factor for ClpXP that controls substrate choice.

Members of the Clp/Hsp100 adenosine triphosphatase (ATPase) family are hexameric, ring-shaped proteins that catalyze the unfolding of specific target proteins (*1*–*8*). Clp/Hsp100-catalyzed unfolding reactions have been implicated in a variety of intracellular processes, including reactivating heat-damaged proteins during stress, modulating the transformation of prionlike factors, and disassembling or degrading protein complexes involved in transposition, DNA replication, and virulence (*9*, *10*). Many family members also participate directly in protein degradation by unfolding proteins and transporting the unfolded chain to an associated peptidase complex. For example, the ClpX unfoldase associates with the ClpP serine peptidase to form the multiring ClpXP protease (*6*, *11*).

Clp/Hsp100 ATPases appear to recognize their substrates by binding to short, unstructured peptide sequences displayed on otherwise native proteins (*12*–*15*). The best characterized recognition peptide is the ssrA tag, AANDENYALAA, which targets proteins to the ClpX and ClpA ATPases (*7*, *8*, *12*). Despite recent progress in identifying substrates for the Clp/Hsp100 proteins and the peptide signals important for their recognition, no simple sequence code has emerged that marks proteins as a specific substrate for a particular unfolding ATPase. Furthermore, although both ClpXP and ClpAP efficiently degrade ssrA-tagged proteins in vitro, ClpXP is largely responsible for degradation of these proteins in the cell (*12*). These observations suggested that additional cellular factors might serve to modulate substrate recognition in vivo.

Initial evidence for a ClpX-stimulatory factor was observed during purification of *Escherichia coli* ClpX, and a high-salt wash of partially purified ribosomes was found to be especially rich in this activity (*16*). Under conditions where purified ClpXP partially degraded green fluorescent protein carrying an ssrA tag (GFP-ssrA) (*17*), this activity stimulated degradation 10 times or more (Fig. 1A). We purified the stimulatory factor (*18*) until a single major protein of ~20 kD was visible by SDS–polyacrylamide gel electrophoresis (SDS-PAGE). NH_2-terminal sequencing identified this protein as SspB (stringent starvation protein B), a molecule of unknown function that is part of an operon induced by starvation (*19*). To demonstrate that SspB was indeed the stimulatory factor, we overproduced the protein (*20*) and purified it to apparent homogeneity (Fig. 1B).

Rates of GFP-ssrA degradation by ClpXP were determined in the presence or absence of SspB (Fig. 1C). SspB reduced the Michaelis constant (K_m) for this substrate by a factor of 4 to 5, indicating that it enhances productive interactions between ClpXP and ssrA-tagged proteins. SspB also stimulated V_{max} by about 25%. Moreover, SspB stimulated degradation over many enzyme turnovers, did not stimulate degradation of other ClpXP substrates (MuA and λ O), and did not stimulate ClpAP, which also recognizes and degrades GFP-ssrA (*7*). Thus, SspB enhances substrate recognition of ssrA-tagged substrates by the ClpX ATPase in a highly specific manner.

SspB bound specifically to ssrA-tagged proteins (*21*) (Fig. 2). SspB and GFP-ssrA coeluted from a Superose 12 column (Fig. 2A), whereas SspB and untagged GFP eluted as distinct peaks (Fig. 2B). Likewise, the ssrA-tagged NH_2-terminal domain of λ repressor (λ-cI-N-ssrA) was bound by SspB (Fig. 2C). Mutagenesis of the ssrA tag revealed that residues critical for SspB binding were distinct from those recognized by ClpX. Mutations in the YALAA portion of the tag did not prevent SspB binding (Fig. 2, D to F) but severely reduced degradation by ClpXP (*8*, *12*). By contrast, the $Asn^3 \rightarrow Ala$ (N3A) mutation in the AANDEN segment of the tag obliterated binding of SspB (Fig. 3A) and eliminated SspB stimulation of ClpXP degradation without affecting unstimulated degradation (Fig. 3B). Thus, Asn^3 in the ssrA tag is a cardinal determinant of SspB recognition, and binding of SspB to the peptide tag is critical for

[1]Department of Biology and [2]Howard Hughes Medical Institute, Building 68, Room 523, Massachusetts Institute of Technology, 77 Massachusetts Avenue, Cambridge, MA 02139, USA.

*To whom correspondence should be addressed. E-mail: tabaker@mit.edu